This is an open access article published under an ACS AuthorChoice License, which permits copying and redistribution of the article or any adaptations for non-commercial purposes.

ACS OMEGA

Article

http://pubs.acs.org/journal/acsodf

Graphene–Metal Composite Sensors with Near-Zero Temperature Coefficient of Resistance

Brandon C. Marin, Samuel E. Root, Armando D. Urbina, Eden Aklile, Rachel Miller, Aliaksandr V. Zaretski, and Darren J. Lipomi*

Department of NanoEngineering, University of California, San Diego, 9500 Gilman Drive, Mail Code 0448, La Jolla, California 92093-0448, United States

Supporting Information

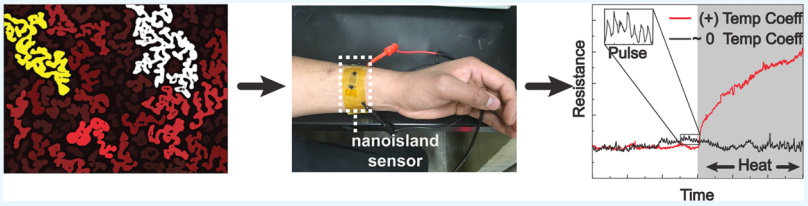

ABSTRACT: This article describes the design of piezoresistive thin-film sensors based on single-layer graphene decorated with metallic nanoislands. The defining characteristic of these composite thin films is that they can be engineered to exhibit a temperature coefficient of resistance (TCR) that is close to zero. A mechanical sensor with this property is stable against temperature fluctuations of the type encountered during operations in the real world, for example, in a wearable sensor. The metallic nanoislands are grown on graphene through thermal deposition of metals (gold or palladium) at a low nominal thickness. Metallic films exhibit an increase in resistance with temperature (positive TCR), whereas graphene exhibits a decrease in resistance with temperature (negative TCR). By varying the amount of deposition, the morphology of the nanoislands can be tuned such that the TCRs of a metal and graphene cancel out. The quantitative analysis of scanning electron microscope images reveals the importance of the surface coverage of the metal (as opposed to the total mass of the metal deposited). The stability of the sensor to temperature fluctuations that might be encountered in the outdoors is demonstrated by subjecting a wearable pulse sensor to simulated solar irradiation.

INTRODUCTION

Wearable and implantable sensors can be designed to detect a range of chemical, biophysical, electromagnetic, and thermal stimuli. However, some types of sensors are responsive only to one type of stimulus. For example, strain gauges based on metallic thin films are sensitive not only to mechanical deformation but also to temperature. Unwanted sensitivity to temperature could arise because of, for example, thermal expansion of the substrate or the fact that the conductivity of a metal depends on temperature (i.e., the temperature coefficient of resistance, TCR). Our laboratory has previously shown that metallic nanoislands on graphene are sensitive to a wide range of mechanical, optical, chemical, and electrophysiological signals.[1,2] During the course of these experiments, we noticed that thermal drift—that is, small changes in the local ambient temperature—produced changes in the electrical resistance of the sensors that were comparable to or greater than those produced by the stimuli of interest. The problem of convoluted signals is not unique to this type of sensor but is rarely reported for experiments on other types of sensors, which are performed in well-controlled environments.

Decoupling the signal of interest from unwanted signals can be addressed in one of at least two ways: (1) by processing the signals using back-end electronics or (2) by designing the material used for sensing. This paper uses the second approach—in which decoupling of thermal drift is accomplished by the material itself. Because graphene exhibits a TCR that is less than zero[3] and metals exhibit a TCR that is greater than zero,[4] we fabricated composite thin films consisting of metallic nanoislands supported by single-layer graphene (Figure 1). (Metallic nanoislands are the disconnected structures that form with low nominal thicknesses when metals are deposited through physical vapor deposition.) By tuning the amount of metals deposited—and thus the interconnectivity and surface coverage of the nanoislands—it was possible to engineer the composite material such that the TCR of the two different materials canceled out to near zero.

Previous work on the topic of zero-TCR materials has been primarily concerned with bulk metal alloys and other materials that require complex processing. Metal alloys include manganin and constantin; the latter has been used for over a century in the components of thermocouples. New alloys[5−7] have been developed, along with tunable-TCR materials such as metal–polymer composites,[8−11] carbon mixtures,[12] and semiconductor composites.[13−15] Optical strain sensors that are temperature-independent have also been reported.[16] However, polymer and

Received: January 12, 2017
Accepted: February 8, 2017
Published: February 21, 2017

 © 2017 American Chemical Society

DOI: 10.1021/acsomega.7b00044
ACS Omega 2017, 2, 626−630

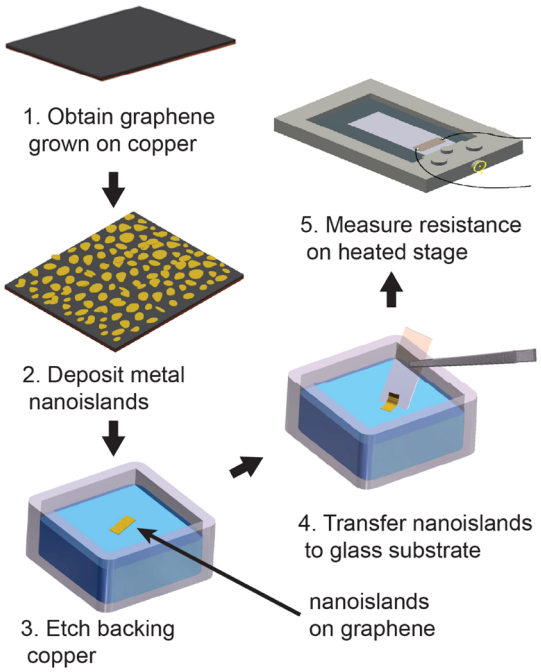

Figure 1. Schematic diagram of the process used to generate and transfer metallic nanoislands on graphene. Nanoislands are formed by thermal evaporation of metals onto copper-supported graphene. The backing copper is etched using a basic ammonium persulfate solution. The film can then be transferred to a substrate of interest and addressed for electrical measurements.

carbon mixtures involve complex solution processing, and metal alloys reported so far have been bulk materials, as opposed to thin films. For near-zero-TCR sensing elements to be useful in flexible and wearable devices, it is desirable to have active materials that are thin, transparent, and mechanically robust.

A single layer of graphene behaves as a zero-gap semiconductor with a negative TCR at room temperature. The resistivity is dominated by the charge-carrier concentration and decreases with temperature as more hot carriers become available.[17] This phenomenon is in contrast to metals, which typically have a positive TCR owing to an increase in both inelastic electron scattering and lattice spacing with temperature.[18] Given our previous experience with metal nanoislands on graphene as a platform for multimodal sensing,[2,19] we hypothesized that a zero-TCR sensor could be fabricated if the right amount of metal was deposited onto the graphene such that the effects of each material cancel each other out. To design this material, we characterized the effect of deposition thickness and island morphology on the TCR of the graphene–metal composites. Gold and palladium were selected as the metals to test this hypothesis because of their widespread use in thermal and chemical thin-film sensing and disparate morphologies formed when evaporated onto graphene.[1,20]

RESULTS AND DISCUSSION

Thermoresistive Behavior of Metal Nanoislands. The relationship between electrical resistance, temperature, and thickness for metal nanoislands on graphene is summarized in Figure 2a (gold) and 2b (palladium). The reported thicknesses are the "nominal" values measured using the quartz crystal microbalance in the evaporation chamber. (The true thickness is poorly defined because of the disconnected nature of the nanoisland films.) To find the TCR of these samples, we

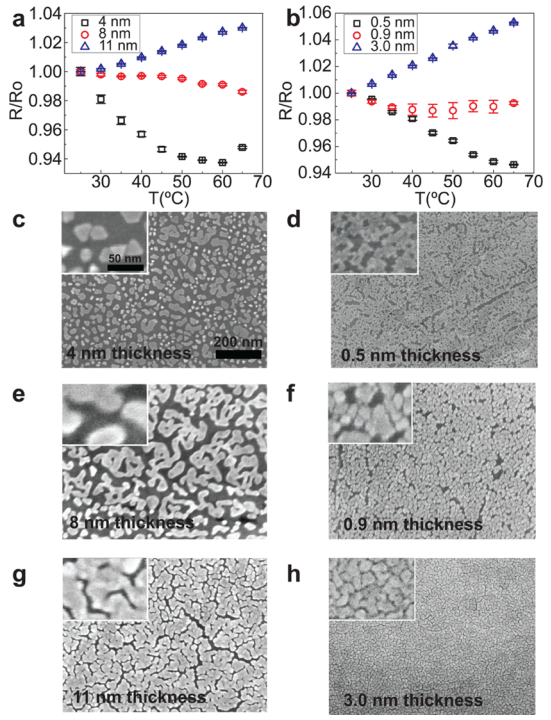

Figure 2. Thermoresistive behavior and morphology of gold and palladium nanoislands. The temperature-dependent normalized resistance is plotted for gold nanoislands (a) and palladium nanoislands (b) of varied nominal thicknesses. SEM micrographs depicting negative-TCR isolated nanoislands for 3 nm of gold (c) and 0.5 nm of palladium (d), near-zero TCR, partially percolated structures for 8 nm of gold (e) and 0.9 nm of palladium (f), and positive TCR, fully percolated structures for 11 nm of gold (g) and 3.0 nm of palladium (h). All SEM images are under the same magnification.

measured the normalized resistance as a function of temperature (from 30 to 65 °C); the TCR is the slope of this curve. As we expected, the TCR of the composite films exhibited a strong dependence on the nominal thickness of the metallic film. The scanning electron microscope (SEM) images shown in Figure 2c–h suggest that the morphology—that is, interconnectivity or fractional surface coverage—also influences the sensitivity to temperature.

The SEM images in Figure 2c,d show distinct differences between the morphologies of the negative-TCR composites of gold and palladium, respectively. At a nominal thickness of 4 nm, the gold assembles into large separated islands with sharp crystalline facets. Palladium nanoislands, in contrast, are smaller than gold nanoislands at all nominal thicknesses. Moreover, they exhibit a higher fractional coverage at substantially lower nominal thicknesses (0.5 nm). It also appears that the palladium nanoislands may be interconnected.

The nominal thickness of deposition that gave near-zero TCR was 8 nm for gold and 0.9 nm for palladium. The SEM image in Figure 2e shows that gold forms partially percolated fractal structures that resulted from isolated nanoislands coalescing in a disordered fashion during the growth process. On the other hand, the palladium nanoislands did not coalesce but did appear to be in intimate physical contact (Figure 2f). We attribute the differences in morphology to the differences in relative interaction energies between the surface and the metal nanoislands: palladium has a stronger attraction to the surface and a closer epitaxial registry (a smaller lattice constant).[21]

DOI: 10.1021/acsomega.7b00044
ACS Omega 2017, 2, 626–630

Therefore, the palladium nanoislands are less mobile than the gold nanoislands during the growth process.[1] The SEM images in Figure 2g,h show that gold and palladium form completely percolated nanostructures with a nominal thickness greater than 11 and 3 nm, respectively. Percolated structures in both materials yielded a positive TCR—evidence that the thermoresistive behavior approaches that of a thin film of metal.

In general, these results show that the TCR can be controlled as a function of nominal thickness of deposition. In cases when it is necessary to eliminate thermal drift, a substrate with a near-zero TCR can be repeatedly fabricated using either palladium or gold by targeting a specific thickness. Moreover, this procedure should be straightforward to transfer to any other transition metal of interest for a specific device application. Interestingly, we found a large difference in the nominal thickness that produced a near-zero TCR of palladium (0.9 nm) versus that of gold (8 nm). Although morphologies can be reproduced by holding the deposition parameters constant (chamber pressure, evaporation rate, substrate, and nominal thickness),[22] the nominal thickness is not a true indication of the thickness of individual nanoislands. Thus, we found it necessary to correlate the TCR with other morphological parameters to give a more sophisticated description of the relationship between the TCR and the morphology of the metal nanoislands.

Image Analysis and Modeling of the Thermoresistive Behavior of Metal Nanoislands. Image analysis was performed on the SEM micrographs of gold nanoislands to quantitatively analyze the trends between morphology and thermoresistive behavior. A thresholding algorithm known as Otsu's method[23] was used to differentiate the metal structures from graphene. The algorithm operates on the grayscale image by assuming two classes of pixels, which fall above or below a threshold value (metal vs graphene). The optimum threshold value is defined as the one that minimizes the variance within each class of pixels. Once differentiated, distinct islands are labeled and various properties are computed including surface coverage and projected area. From Figure 3a, we can see that TCR varies linearly with coverage. Examples of processed images are given in Figure 3b–d, where the separate islands are colored by their area.

Given the observed dependence of TCR with coverage, we developed a model to describe the thermoresistive behavior of this composite material. Adomov et al.[24] have demonstrated that the TCR of vacuum-deposited gold films depends on thickness, d, and can be described as

$$\alpha_{Au} = \alpha_o\left(1 + \frac{3l}{8d}\right)^{-1}$$

where α_{Au} is the TCR of gold and l is the electron mean free path (400 Å). The actual island thickness can be related to the nominal thickness using the coverage, θ, and the following relation

$$d = \frac{d^*}{\theta}$$

Finally, the TCR of the gold islands can be combined with the TCR of the supporting graphene (α_{Gr}) using a composite theory, with coverage as the fractional variable

$$\alpha_c = \theta\alpha_{Au} + (1 - \theta)\alpha_{Gr}$$

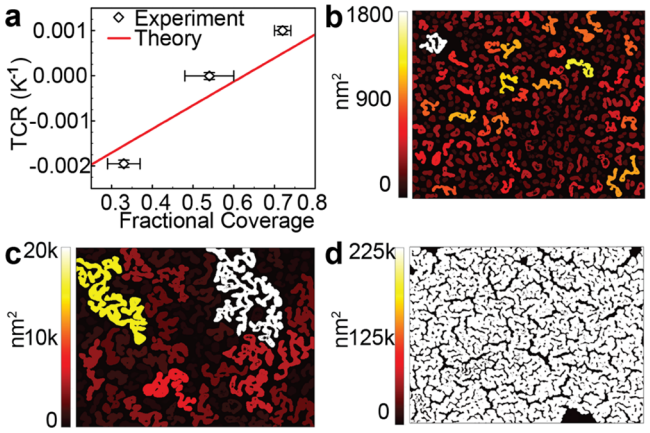

Figure 3. Morphological dependence of the TCR of gold nanoislands obtained through image analysis. (a) Plot showing linear dependence of TCR on fractional coverage. Representative processed images for (b) negative TCR (4 nm), (c) near-zero TCR (8 nm), and (d) positive TCR (11 nm) gold nanoislands. Islands are colored by the projected area (nm^2). The film in (d) is entirely white because it is a single interconnected structure of area 225k nm^2.

The results of our model are compared with the experimental data in Figure 3a and demonstrate good agreement. Additional details on the composite model are available in the Supporting Information.

The results of our model suggested that the lateral distribution of the metal was more important than the total mass deposited. To test this idea, we subjected an 11 nm gold nanoisland sample to rapid thermal annealing (RTA), a method that has commonly been used to change the morphology of metallic films on the nanoscale.[25,26] The sample was heated from room temperature to 600 °C in 12 s and held at the elevated temperature for 5 min. This thermal treatment changed the morphology of the metal from a percolated network to a distribution of isolated nanoparticles (Figure S3). The TCR of the sample changed concomitantly from positive to negative (Figure S4). This experiment unambiguously demonstrated the importance of interconnectivity and surface coverage of the metal islands on the TCR of the composite material.

Wearable Application of Sensors with Near-Zero TCR. To demonstrate the utility of thin films resistant to thermal drift, we fabricated a wearable sensor for detecting the human pulse using gold nanoislands. Nanoisland-graphene films with positive, negative, and near-zero TCRs were transferred onto Kapton tape, addressed with carbon paint, and then adhered onto the wrist, as depicted in Figure 4a. A schematic diagram of the sensor is shown in Figure S7. To simulate a plausible real-world scenario where an abrupt heating event would occur, we placed the sensor (on the wrist) over a solar simulator lamp to imitate the direct illumination of a sensor by the sun. As indicated by the gray-shaded area in Figure 4b, the gold nanoislands with the near-zero TCR exhibited a minimal thermal drift. On the other hand, the positive- and negative-TCR sensors experienced a substantial drift owing to heating caused by direct illumination. When placed on the wrist, periodic strain caused by the contractions of the radial artery induced a periodic change in resistivity. This pulse signal was detected by the sensor (inset Figure 4b). To address whether the sensitivity of the wearable sensor was affected by changing the nominal thickness of the metal to attain a near-zero TCR,

DOI: 10.1021/acsomega.7b00044
ACS Omega 2017, 2, 626–630

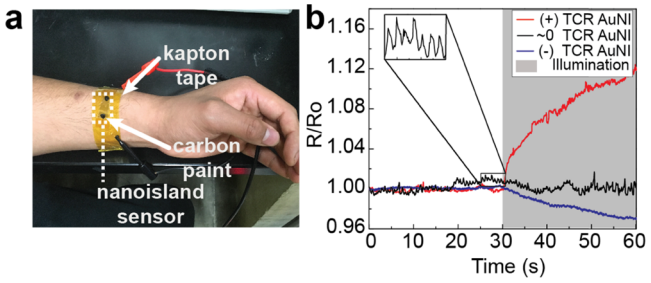

Figure 4. Thermal drift of a wearable pulse sensor under simulated sunlight. (a) Wearable pulse sensor with the nanoisland portion outlined in black dashed lines. (b) Normalized resistance is plotted versus time with a period of illumination by a solar simulator lamp, which is marked by the gray-shaded area. The lamp heated the sensor to a steady-state temperature of approximately 45 °C after 30 s as measured using an infrared thermometer. The inset shows a clear pulse, with dicrotic notches clearly visible.

we examined the data closely in Figure 4b. Assuming that the strain caused by a pulse was constant (because the same subject was used for all measurements in Figure 4b), the pulse signal was most pronounced in the near-zero-TCR sensor, indicating that the sensor performance was not diminished by changing the nominal thickness of metals. We then tested for any possible interference from temperature-dependent conductivity of the carbon paint itself. We attached copper wires to a gold film (50 nm) using a drop of carbon paint with similar dimensions to those used in the wearable sensors. Continuous measurement of resistance as a function of temperature from ambient temperature to 60 °C revealed a net increase in resistance of <1%. Given this small effect and the fact that the samples were all connected using the same materials, we can confirm that the observed differences in TCR between the graphene-nanoisland films were due to the coverage and interconnectivity of the nanoislands.

CONCLUSIONS

We reported a new strategy to suppress thermal drift in sensors. This strategy is based on the precise control of materials in sensors composed of graphene decorated with metal nanoislands. By systematically varying the nominal thickness of the metal deposited, we found optimal deposition parameters to produce composite thin films with near-zero TCR for both gold and palladium on graphene. Differences in the self-assembly process of gold nanoislands suggested that surface coverage and interconnectivity were the most important morphological parameters in determining the TCR of the composite material. Image analysis of SEM images provided quantitative evidence to support this conclusion and enabled the development of a model to describe the thermoresistive behavior of the composite material. Proof-of-concept wearable sensors were fabricated to demonstrate the stability of the electrical signal to variations in surface temperature produced by sunlight. This material-design strategy should be easily generalizable to other transition metals for device-specific applications (e.g., chemical sensing) and provides a robust platform for the development of devices that minimize fluctuations due to temperature. More generally, these experiments demonstrate how well-known materials can be combined in new ways to design thin-film composites with useful properties for device applications.

EXPERIMENTAL SECTION

Metal Nanoisland Sensor Fabrication. Metal nanoislands were fabricated by physical vapor deposition using an AJA International thermal evaporator (Orion-class). A thin film of palladium or gold was deposited onto graphene supported on copper foil at a rate of 0.05 Å/s. Chamber pressure during deposition was 2.0×10^{-7} Torr. The resultant structure comprised nanoislands on graphene on copper foil (nanoisland/Gr/Cu). Poly(methylmethacrylate) (PMMA) (1 kDa, 200 nm) was spin-coated (1 wt % solution in anisole at 4k rpm for 60 s) onto the nanoisland side of the nanoisland/Gr/Cu sample. The backing copper foil was etched by floating the sample copper-side-down in an aqueous ammonium persulfate solution (50 mg/mL) for approximately 3 h. The samples were then transferred onto a 1 in. × 3 in. glass slide. The PMMA layer was then dissolved using neat acetone at 40 °C.

SEM. An FEI XL30 SFEG instrument with an FEI Sirion column and Through-Lens Detector was used for SEM micrographs of metal nanoislands. An accelerating voltage of 10 kV and a spot of 50 μm were used for imaging.

TCR Measurements. Resistance measurements were recorded using a Keithley 2400 sourcemeter. All resistance measurements for wearable applications and TCR calculations were conducted using two-point measurements. To decouple the possible effects of the contact resistance of the carbon paint from the intrinsic resistance of the graphene-nanoisland films, we compared the resistances obtained using two-point measurements to those obtained using four-point measurements. The fact that the resistance values differed by less than 1% suggested that the contact resistance due to the carbon paint was negligible. All samples had the same dimensions. The samples for TCR measurements were heated using an Instec FS1 heating stage with an Instec mK2000 temperature controller and electrically addressed with eutectic gallium–indium (EGaIn).

Image Analysis. An object-oriented Python code was developed to perform image analysis of the SEM images. This code made extensive use of the Mahotas package (see Supporting Information) to distinguish the metal from graphene, identify separate nanoislands, and quantify the area of the individual nanoislands as well as their fractional coverage over the graphene. The code can be easily adapted for the analysis of similar nanostructures and is openly available at github.

RTA. RTA was performed using an AG Associates Heatpulse 610. The samples were heated from room temperature to 600 °C in 12 s (50 °C/s) under forming gas (5% hydrogen/95% nitrogen) to aid reflow of the metal. The sample was held at the elevated temperature for 5 min.

ASSOCIATED CONTENT

Supporting Information

The Supporting Information is available free of charge on the ACS Publications website at DOI: 10.1021/acsomega.7b00044.

Additional thermoresistive data for gold and palladium nanoislands, SEM micrographs of and thermoresistive data for gold nanoislands before and after RTA, image analysis description, composite model description, and schematic drawing of the wearable sensor (PDF)

DOI: 10.1021/acsomega.7b00044
ACS Omega 2017, 2, 626–630

AUTHOR INFORMATION

Corresponding Author

*E-mail: dlipomi@eng.ucsd.edu (D.J.L.).

ORCID

Darren J. Lipomi: 0000-0002-5808-7765

Notes

The authors declare no competing financial interest.

ACKNOWLEDGMENTS

This work was supported by the National Institutes of Health Director's New Innovator Award, grant 1DP2EB022358-01 to D.J.L., and by a Diversity Supplement (for B.C.M.) under the same award number. E.A. received partial support from the CA-NASA/UCSD Space Grant Consortium. This work was performed in part at the San Diego Nanotechnology Infrastructure (SDNI), a member of the National Nanotechnology Coordinated Infrastructure, which is supported by the National Science Foundation (grant ECCS-1542148).

REFERENCES

(1) Zaretski, A. V.; Root, S. E.; Savchenko, A.; Molokanova, E.; Printz, A. D.; Jibril, L.; Arya, G.; Mercola, M.; Lipomi, D. J. Metallic Nanoislands on Graphene as Highly Sensitive Transducers of Mechanical, Biological, and Optical Signals. *Nano Lett.* **2016**, *16*, 1375−1380.

(2) Marin, B. C.; Liu, J.; Aklile, E.; Urbina, A. D.; Chiang, A. S.-C.; Lawrence, N.; Chen, S.; Lipomi, D. J. SERS-Enhanced Piezoplasmonic Graphene Composite for Biological and Structural Strain Mapping. *Nanoscale* **2017**, *9*, 1292−1298.

(3) Shao, Q.; Liu, G.; Teweldebrhan, D.; Balandin, A. A. High-Temperature Quenching of Electrical Resistance in Graphene Interconnects. *Appl. Phys. Lett.* **2008**, *92*, 202108.

(4) Mott, N. F. The Resistance and Thermoelectric Properties of the Transition Metals. *Proc. R. Soc. London, Ser. A* **1936**, *156*, 368−382.

(5) Yi, L.; Jiao, W.; Zhu, C.; Wu, K.; Zhang, C.; Qian, L.; Wang, S.; Jiang, Y.; Yuan, S. Ultrasensitive Strain Gauge with Tunable Temperature Coefficient of Resistivity. *Nano Res.* **2016**, *9*, 1346−1357.

(6) Neugebauer, C. A.; Webb, M. B. Electrical Conduction Mechanism in Ultrathin, Evaporated Metal Films. *J. Appl. Phys.* **1962**, *33*, 74−82.

(7) Fu, B.; Gao, L. Tantalum Nitride/Copper Nanocomposite with Zero Temperature Coefficient of Resistance. *Scr. Mater.* **2006**, *55*, 521−524.

(8) Lee, S.-E.; Sohn, Y.; Chu, K.; Kim, D.; Park, S.-H.; Bae, M.; Kim, D.; Kim, Y.; Han, I.; Kim, H.-J. Suppression of Negative Temperature Coefficient of Resistance of Multiwalled Nanotube/Silicone Rubber Composite through Segregated Conductive Network and Its Application to Laser-Printing Fusing Element. *Org. Electron.* **2016**, *37*, 371−378.

(9) Pang, H.; Zhang, Y.-C.; Chen, T.; Zeng, B.-Q.; Li, Z.-M. Tunable Positive Temperature Coefficient of Resistivity in an Electrically Conducting Polymer/Graphene Composite. *Appl. Phys. Lett.* **2010**, *96*, 251907.

(10) Pang, H.; Chen, C.; Bao, Y.; Chen, J.; Ji, X.; Lei, J.; Li, Z.-M. Electrically Conductive Carbon Nanotube/Ultrahigh Molecular Weight Polyethylene Composites with Segregated and Double Percolated Structure. *Mater. Lett.* **2012**, *79*, 96−99.

(11) Li, G.; Hu, C.; Zhai, W.; Zhao, S.; Zheng, G.; Dai, K.; Liu, C.; Shen, C. Particle Size Induced Tunable Positive Temperature Coefficient Characteristics in Electrically Conductive Carbon Nanotubes/Polypropylene Composites. *Mater. Lett.* **2016**, *182*, 314−317.

(12) Sun, P.; Zhu, M.; Wang, K.; Zhong, M.; Wei, J.; Wu, D.; Zhu, H. Small Temperature Coefficient of Resistivity of Graphene/Graphene Oxide Hybrid Membranes. *ACS Appl. Mater. Interfaces* **2013**, *5*, 9563−9571.

(13) Lin, J. C.; Wang, B. S.; Tong, P.; Lin, S.; Lu, W. J.; Zhu, X. B.; Yang, Z. R.; Song, W. H.; Dai, J. M.; Sun, Y. P. Tunable Temperature Coefficient of Resistivity in C- and Co-Doped $CuNMn_3$. *Scr. Mater.* **2011**, *65*, 452−455.

(14) Lin, S.; Wang, B. S.; Lin, J. C.; Huang, Y. N.; Lu, W. J.; Zhao, B. C.; Tong, P.; Song, W. H.; Sun, Y. P. Tunable Room-Temperature Zero Temperature Coefficient of Resistivity in Antiperovskite Compounds $Ga_{1-x}CFe_3$ and $Ga_{1-y}Al_yCFe_3$. *Appl. Phys. Lett.* **2016**, *101*, 011908.

(15) Bonavolontà, C.; Camerlingo, C.; Carotenuto, G.; De Nicola, S.; Longo, A.; Meola, C.; Boccardi, S.; Palomba, M.; Pepe, G. P.; Valentino, M. Characterization of Piezoresistive Properties of Graphene-Supported Polymer Coating for Strain Sensor Applications. *Sens. Actuators, A* **2016**, *252*, 26−34.

(16) Lee, S.; Lim, E. J.; Jo, I. S.; Yoo, K. W.; Han, Y. Temperature-Insensitive Strain Sensor Using a Microfiber Mach-Zehnder Interferometer. In *Asia-Pacific Optical Sensors Conference*, OSA Publishing | The Optical Society, 2016; Vol. 2, pp 3−5.

(17) Geim, A. K.; Novoselov, K. S. The Rise of Graphene. *Nat. Mater.* **2007**, *6*, 183−191.

(18) Shivaprasad, S. M.; Angadi, M. A. Temperature Coefficient of Resistance of Thin Palladium Films. *J. Phys. D: Appl. Phys.* **1980**, *13*, L171.

(19) Zaretski, A. V.; Lipomi, D. J. Processes for Non-Destructive Transfer of Graphene: Widening the Bottleneck for Industrial Scale Production. *Nanoscale* **2015**, *7*, 9963−9969.

(20) Zaretski, A. V.; Marin, B. C.; Moetazedi, H.; Dill, T. J.; Jibril, L.; Kong, C.; Tao, A. R.; Lipomi, D. J. Using the Thickness of Graphene to Template Lateral Subnanometer Gaps between Gold Nanostructures. *Nano Lett.* **2015**, *15*, 635−640.

(21) Buch, A. *Pure Metals Properties: A Scientific and Technical Handbook*, 1st ed.; ASM International: Materials Park, OH, 1999.

(22) Mattox, D. M. *Handbook of Physical Vapor Deposition (PVD) Processing*, 2nd ed.; Elsevier: Oxford, 2010.

(23) Otsu, N. A Threshold Selection Method from Gray-Level Histograms. *Automatica* **1979**, *11*, 23−27.

(24) Adamov, M.; Perović, B.; Nenadović, T. Electrical and Structural Properties of Thin Gold Films Obtained by Vacuum Evaporation and Sputtering. *Thin Solid Films* **1974**, *24*, 89−100.

(25) Jia, K.; Bijeon, J.-L.; Adam, P.-M.; Ionescu, R. E. Large Scale Fabrication of Gold Nano-Structured Substrates via High Temperature Annealing and Their Direct Use for the LSPR Detection of Atrazine. *Plasmonics* **2012**, *8*, 143−151.

(26) Strekal, N.; Maskevich, A.; Maskevich, S.; Jardillier, J.-C.; Nabiev, I. Selective Enhancement of Raman or Fluorescence Spectra of Biomolecules Using Specifically Annealed Thick Gold Films. *Biopolymers* **2000**, *57*, 325−328.

DOI: 10.1021/acsomega.7b00044
ACS Omega 2017, 2, 626−630